Article

Investigation of Parking Lot Pavements to Counteract Urban Heat Islands

Laura Moretti [1,*] , **Giuseppe Cantisani** [1] , **Marco Carpiceci** [2] , **Antonio D'Andrea** [1] , **Giulia Del Serrone** [1] , **Paola Di Mascio** [1] , **Paolo Peluso** [1] **and Giuseppe Loprencipe** [1]

1   Department of Civil, Constructional and Environmental Engineering, Sapienza University of Rome, Via Eudossiana 18, 00184 Rome, Italy; giuseppe.cantisani@uniroma1.it (G.C.); antonio.dandrea@uniroma1.it (A.D.); giulia.delserrone@uniroma1.it (G.D.S.); paola.dimascio@uniroma1.it (P.D.M.); paolo.peluso@uniroma1.it (P.P.); giuseppe.loprencipe@uniroma1.it (G.L.)
2   Department of History, Representation and Restoration of Architecture, Sapienza University of Rome, Piazza Borghese 9, 00186 Rome, Italy; marco.carpiceci@uniroma1.it
*   Correspondence: laura.moretti@uniroma1.it; Tel.: +39-06-44585114

Abstract: Urban heat islands (UHI) are one of the unequivocal effects of the ongoing process of climate change: anthropized areas suffer extreme heat events that affect the human perception of comfort. This study investigated the effects of road pavements as a passive countermeasure by comparing the air temperature (AT) and the predicted mean vote (PMV) for different surface materials used to pave a historical square in Rome, Italy. The software ENVI-met has been used to compare, for the whole year 2021, the performances of the existing asphalt pavement with five alternative solutions composed of light concrete, bricks, stone, wood, and grass. This paper proposed a new methodology to summarize the multi-dimensional results over both temporal and spatial domains. The results of the simulations in the evening of the hottest month showed the existing asphalt pavement gives the worst performance, while the light concrete blocks and the grass pavement ensure the coolest solutions in terms of AT (the average AT is 32 °C for the asphalt pavement and 30 °C for the modular one) and PMV (the maximum PMV value is 4.6 for the asphalt pavement and 4.4 for the modular and grass ones).

Keywords: urban heat island; cool pavements; ENVI-met; concrete pavers; air temperature; asphalt; predicted mean vote

1. Introduction

The ongoing climate changes and the increasing global warming are a process harmful to the earth whose causes should be identified and then mitigated, if not eliminated [1,2]. One of these is certainly man, who, through his socio-political actions, is responsible for climate change [3]. Different studies have shown the critical importance of man on energy consumption due to the urbanization of rural areas and the configuration of urban areas [4]. Several variables (e.g., building size, population density, plant cover, and surface colors) have a significant impact on the amount of used and consumed energy [5,6]. The anthropogenic forcing of land use contributes to the formation of urban heat islands (UHIs) [6]. The heating associated with UHIs is mainly due to the replacement of natural surfaces with waterproof ones, which absorb heat during the day and release it during the night [7–9]. Therefore, the greater heat accumulation in urban areas compared to the surrounding rural areas contributes significantly to the formation of UHIs, in which air temperatures are higher from about 1 °C to over 10 °C [6,10–12]. This negatively affects both the environment and livability due to the increased energy demand and the emissions into the air [13,14]. The main difference between urban and rural areas is the presence of green areas and the materials used [7,15]. The main materials used in anthropized areas, such as

asphalt for roads and concrete for buildings, have physical properties that raise the heating of the urban fabric. In particular, asphalt road pavements, which cover at least 40% of urban areas [16], play a key role in their physical properties [7,17,18]. The two main properties of asphalt are the albedo and emissivity [10,13]: the former is the ability to reflect the solar energy and influences the maximum temperatures, and the latter is the ability to radiate energy or emit energy by radiation and affects the minimum temperatures. Specifically, asphalt has low albedo and high emissivity values [13,19]. The implementation of green urban infrastructures (UGIs) is a way to reduce the impact of UHIs; the introduction of green roofs and facades, green corridors, and green networks can help reduce the temperature in urban areas and offer several advantages, such as pollution reduction and biodiversity safeguarding [20–23]. Compared to the construction of new green areas, the realization of the UGI is less invasive, as a coating with a vegetal layer of the existing surfaces would achieve the benefits related to the increase of evapotranspiration and the consequent cooling of the environment [24,25]. Consequently, there would be reductions in the surface temperatures of buildings, improving the quality of human life. Environmental problems caused by urban heat islands can also be solved by implementing horizontal cool technologies in areas with less stringent structural requirements (e.g., parking lots, parks, or low-traffic roads) [26,27]. Cool pavements are made by replacing the asphalt with cold materials, that is, materials with high values of both albedo and emissivity [28–30].

Cool pavements can be obtained by adopting different strategies [6,7,11,16,31]:

- Reflective pavements: lighter and less rough pavements raise the value of the albedo than ordinary ones, contributing to the reduction of the perceived temperature. Indeed, these strategies allow for the reduction of the amount of absorbed heat, while the reflection increases. The application of light high-reflectance paints and the use of proper materials (e.g., clear concrete and stone) would have a beneficial effect on reducing surface temperatures in urban areas [32,33].
- Porous pavements are composed of porous materials where water moves, affecting the external environmental conditions. The evaporation process of the water stored in the voids during rainy events subtracts heat from the pavement; thus obtaining the beneficial effect of reducing the surface temperature [32,34,35].
- Stone pavements are composed of stone pavers, mainly of light color; the efficient laying pattern with gaps between the blocks ensures the pavement permeability, resulting in one of the most effective cooling methods [36,37].
- Grass pavements integrate interlocking elements and green areas with grass to obtain a significant reduction in surface temperature during daytime hours. Although the grass has a low albedo [38], the absorbed energy allows its perspiration and evapotranspiration. In addition, the turf above the ground reduces the heating of the soil itself by exposure to direct solar radiation, leaving the soil with a greater capacity to absorb thermal energy from the pavers [39].

These listed strategies are the solution admitted by the recent Italian Standard for the promotion of the sustainable public procurement [40]. Such measures are mandatory for all public construction contracts, both in new construction and renovation of existing facilities. Reinforced grass, bricks, light stone, wood, gravel, and permeable pavers should be employed to build road pavements and counteract urban heat islands. This study assesses how microclimatic conditions varied throughout the year 2021 in a parking area, replacing the existing asphalt pavement with different cool pavements to reduce UHI. The dynamic simulation tool ENVI-met 4.3 LITE [41,42] enabled a comparative analysis of various mitigation solutions. The survey was carried out for St. Peter in Chains' square, located in the historic center of Rome, in the Monti district. Taking into account the street planning restrictions and landscaping, five different cool pavements have been modeled to assess their mitigation effects in terms of air temperature and predicted mean vote [41–43]. The authors chose AT and PMV to investigate the representativeness of thermal comfort because such indices are currently used in the literature to analyze outdoor spaces or urban neighborhoods [44–47].

2. Materials and Methods

Albedo and emissivity are the two main parameters that affect the thermal behavior of road pavements [13,48]. Albedo ranges between 0 and 1; the minimum value represents the case of an ideal black surface without reflection that absorbs all the incident radiation, while the maximum value corresponds to a white surface that reflects all the incident radiation [49]. Emissivity is the ability of a material to radiate energy in the form of thermal radiation, estimated as the fraction of energy radiated by that specific material versus the energy radiated by a black body at the same temperature. Emissivity also assumes values between 0 and 1; only a black body has emissivity equal to 1, while any other real object has an emissivity value less than the unit. Therefore, both variables can influence the choice of the correct pavement to counteract UHIs [13]. To date, the most widely used building materials for road pavements have low albedo and high emissivity values. Such physical properties cause, in temperate zones, high surface temperatures of up to 48–67 °C [13,50,51].

In this study, the microclimatic investigation was carried out for St. Peter in Chains' square in Rome (lat. 41°53′36.8″–lon. 12°29′32.1″) where the current state presents two different road pavements (Figure 1).

Figure 1. St. Peter in Chains' square, Rome, Italy.

In the West sector, the parking area has an asphalt pavement, while sampietrini traditional pavers are in the rest of the square. Table 1 shows the physical characteristics of the existing pavement materials [52,53].

Table 1. Physical characteristics of the existing pavement materials.

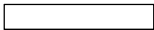| Material	Albedo (-)	Emissivity (-)	Color in Figure 2
Asphalt	0.2	0.9	▬
Sampietrini	0.4	0.9	▬

According to Table 1, the asphalt properties may favor the negative effects of UHI. Five different materials have been proposed to replace the asphalt in the parking area; Table 2 lists their albedo and emissivity values that are suitable to obtain a cool pavement.

Table 2. Physical properties of the modeled cool pavements.

Material	Albedo (-)	Emissivity (-)	Color in Figure 2
Light Concrete	0.8	0.9	▭
Bricks	0.5	0.9	▭
Granite	0.4	0.9	▭
Wood	0.8	0.9	▭
Grass	0.2	(Transmittance 0.3)	▭

This research has been carried out using the software ENVI-met 4.2 LITE (ENVI-met GmbH, Essen, Germany) [36], which performs a microclimatic analysis to assess the urban thermal environment [54]. The software is planned on four different levels. The first layer consists of three main input interfaces that converge in the second layer of the simulation model, which performs the global analysis with computational models and returns the output files (third level). Finally, the last level consists of reading and analysis of the results through two different outputs: the tool Leonardo provides a graphical interface to read, view, and analyze the output data of the simulations [54,55], instead, the tool Xtract allows the extraction of binary output files for ASCII files [42,56].

The study area is defined by several cells of a grid. The current scenario of the square has been modeled with ENVI-met, creating a grid with a resolution of 2 m × 2 m × 2 m (x, y, z) (Figure 3). The ENVI-met model was composed of a one-dimensional (1D) boundary model, a main three-dimensional (3D) model, and a soil model. Local meteorological parameters, different road surfaces, building layouts, vegetation, and soil type constitute the input data necessary to carry out the survey analysis [57]. The interface of ENVI-met Leonardo allows for the reading of the output files, about the different investigated themes and information, through two-dimensional (2D) colored maps.

In addition to the existing scenario, five different scenarios were defined in the ENVI-met software. They differ in the pavement material used for the parking lot in the West area. Table 2 lists the physical properties of the modeled cool materials, which show a higher albedo value than asphalt to obtain climate benefits. Figure 2a–f shows the six analyzed scenarios:

1. First Scenario (BI) is the current layout, where asphalt and sampietrini compose the pavement of the parking and the carriageway, respectively (Figure 2a);
2. Second Scenario (LC): a set of light concrete blocks replaces the asphalt surface in the square (Figure 2b);
3. Third Scenario (BR) is a succession of yellow bricks that substitute the asphalt surface (Figure 2c);
4. Fourth Scenario (SP): a granite pavement substitutes the asphalt surface (Figure 2d);
5. Fifth Scenario (WO): a wooden pavement substitutes the asphalt surface (Figure 2e);
6. Sixth Scenario (GR): a green layer, composed of a small thickness of grass, substitutes for the asphalt surface (Figure 2f).
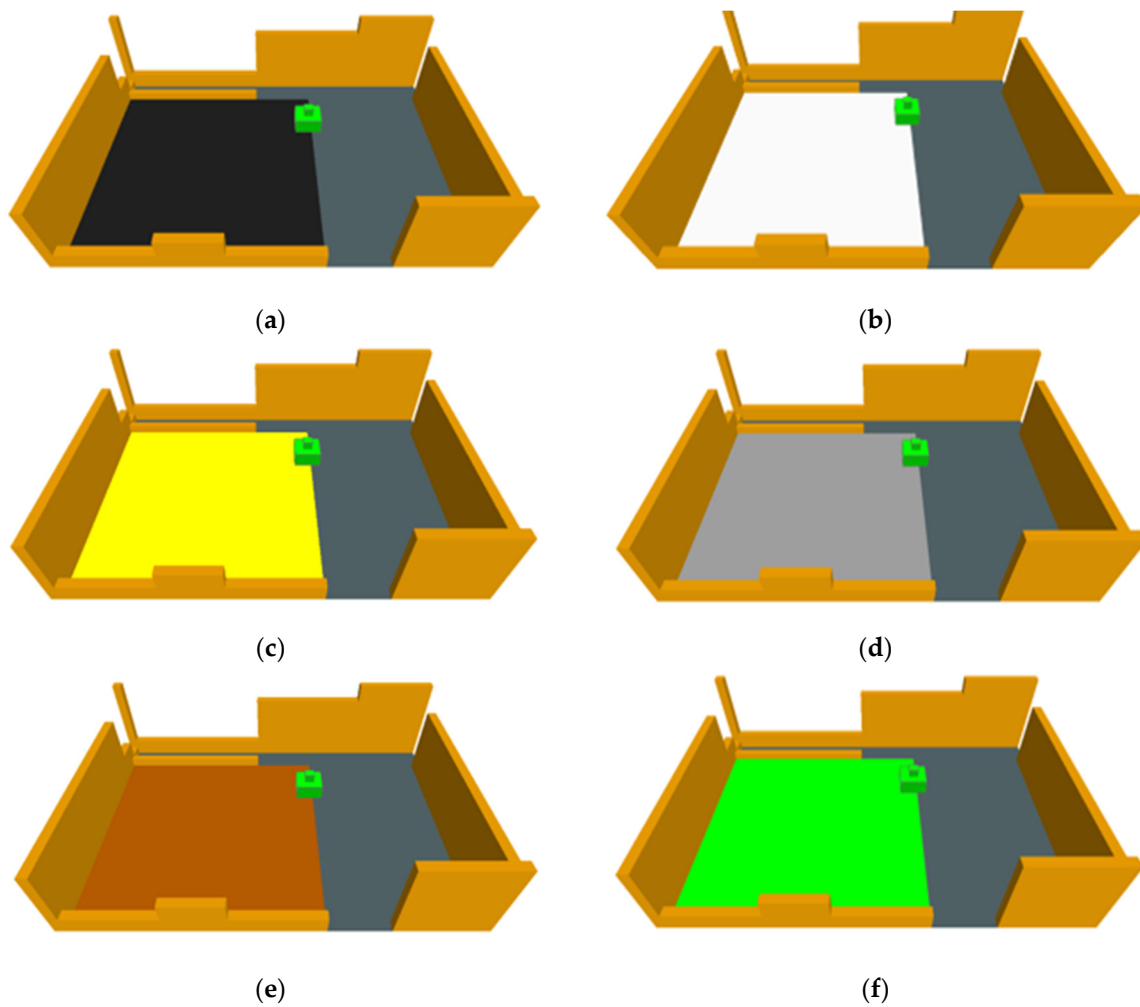
Figure 2. Scenarios implemented and analyzed in ENVI-met: (**a**) First Scenario (BI); (**b**) Second Scenario (LC); (**c**) Third Scenario (BR); (**d**) Fourth Scenario (SP); (**e**) Fifth Scenario (WO); (**f**) Sixth Scenario (GR).

Figure 3. ENVI-met model of St. Peter in Chains' square with grid and boundaries [42].

The simulation, carried out through the software ENVI-met, requires the definition of the temporal period of analysis as input data. The comparison between the different cool pavements replacing the existing one and the evaluation of the thermal effects were implemented for the whole year of 2021. For each analyzed scenario, 12 simulations were executed, one for each month of the year. Each month was defined with 3 days of analysis. The choice of performing a 72 h analysis was made to minimize the spinning effect and to achieve a state of equilibrium in the simulation. Finally, for the elaboration of the results, it was necessary to set among the input data the personal parameters of an average man affected by the climatic effects. In this study a 35-year-old man was considered, he is 1.75 m tall and 75 kg weight.

Table 3 lists the climate input data for each month from the historical meteorological archives. The temperature values are the average ones of the maximum and minimum temperatures. Moreover, a wind speed of 3 m/s and its West direction have been assumed constant during the simulation period.

Table 3. Input data in the ENVI-met simulation model.

Month	T_{min} (°C)	T_{max} (°C)
January	4	11
February	6	15
March	5	15
April	8	17
May	13	22
June	18	29
July	21	32
August	22	32
September	18	19
October	12	22
November	10	17
December	5	13

The ENVI-met Leonardo application tool elaborates colored two-dimensional maps to compare the simulated scenarios [28,55]. The results from the simulations provide different climatic parameters to investigate; according to the scientific literature [58–62], this study focused the attention on the air temperature (AT) and predicted mean vote (PMV). The AT output values of BI have been compared to the experimental measurements taken by the authors in February 2022, July 2021, and October 2021. The measurement process complied with the ISO 7726 standard [63]; the weather station recorded air temperature, relative humidity, and wind speed with a sampling time of 1 min. Table 4 lists the accuracy, resolution, and measurement range of the sensors.

Table 4. Input data in the ENVI-met simulation model.

Climatic Variable	Accuracy	Uncertainty	Measurements Range
Air temperature	0.15 °C at 0 °C	0.1 °C	−10 °C to 80 °C
Relative humidity	±2% (15% to 90%) ±2.5% remaining range	0.1%	5% to 98%
Wind speed	±0.05 m/s (0 m/s to 1 m/s) ±0.15 m/s remaining range	0.01 m/s	0 m/s to 5 m/s

The comparison between the measured and simulated values allowed us to validate the model [64]. Table 5 shows the statistical analysis of all of the collected environmental variables in terms of root mean square error (RMSE).

**Table 5.** Input data in the ENVI-met simulation model.

Climatic Variable	RMSE		
	July 2021	October 2021	February 2022
Air temperature	0.12 °C	0.14 °C	0.16 °C
Relative humidity	15.4%	18.8%	19.3%
Wind speed	0.42 m/s	0.57 m/s	0.62 m/s

PMV is the most widely used thermal comfort index [65] because it allows for the correlation between thermal comfort and meteorological parameters; it depends on air temperature, average radiant temperature, wind speed, humidity, clothing, and activity level [66,67]. Specifically, the American Society of Heating, Refrigerating and Air-Conditioning Engineers (ASHRAE) [68] has developed Equation (1) for the calculation of the dimensionless metric PMV:

$$\begin{aligned} PMV = (0.303exp &- 0.0336M + 0.028) \times \{(M - W) - 3.5 \times 10^{-3} \times [\, 5733 - 6.99 \times (M - W) - p_a\,] - 0.42 \\ &\times (M - 58.5) - 1.7 \times 10^{-5} \times M \times (5867 - p_a) - 0.0014 \times M \times (34 - t_a) - 3.96 \times 10^{-8} \times f_{cl} \times \\ &[(t_{cl} + 273)^4 - (t_r + 273)^4\,] - f_{cl} \times h_c \times (t_{cl} - t_a\} \end{aligned} \quad (1)$$

where M is the metabolism rate, W is the external work, p_a is the partial water vapor pressure (Pa), t_a is the air temperature (°C), f_{cl} is the surface area factor of clothing, t_{cl} is the surface temperature of clothing (°C), t_r is the mean radiant temperature (°C), and h_c is the convective heat transfer coefficient (W/(m^2 × K)). According to the ergonomic standard UNI EN ISO 7730:2006 [69], PMV allows for ex-ante and ex-post analyses for evaluation, design, and control of thermal environments because it summarizes physical and physiological parameters [70] to represent the state of human comfort.

The PMV index in the range +1/−1 represents the ideal condition (IC), considered a comfort zone; the values beyond the range +/− 3 refer to climate scenarios characterized by strong stress situations from the summer heat or winter cold (CC) (Figure 4). The areas between IC and CC identify acceptable conditions (AC).
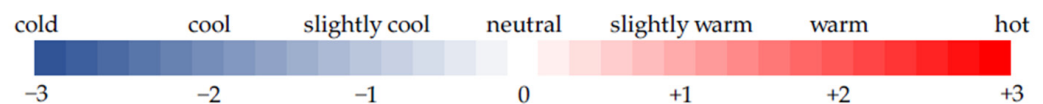
Figure 4. PMV Scale [42].

Since the area of study is exposed to the public for the whole year, the identification of the scenario able to guarantee the best thermal comfort was conducted with an analysis of the PMV, observing and studying the different values it assumes in the cold and hot critical months. Figure 5 shows an extreme trend of a PMV curve of 24 h because there are both hot and cold critical conditions. Figure 5 highlights, colorfully, all of the conditions in Figure 4, according to the PMV values given by Equation (1).

In this study, the different colored areas in Figure 5 have been considered to identify the best pavement from the PMV curve of the two hottest and coldest months. The authors assessed the blue and red areas between the PMV curve and the x-axis to compare the different simulated scenarios; the best scenario has the smallest dark blue and red areas.
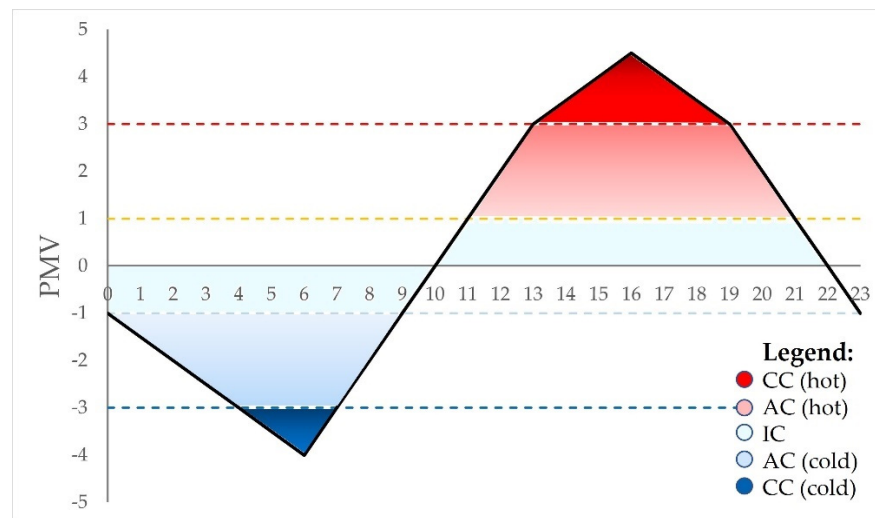
Figure 5. Example of an extreme daily trend of the PMV.

3. Results

Figure 6 shows the layout of the ENVI-met models: the area is bounded by buildings and walls (red lines in Figure 6 corresponding to the red lines in Figure 3) except for the road cross-sections off the carriageway through the square. The study deepened the thermal performances of 9 points (P_i, i = 1, ... , 9) in the parking area, where, to date, there is a tree (green area in Figure 6). P_5 is the barycenter of the parking area while the other ones are on the boundaries of the maneuvering area.
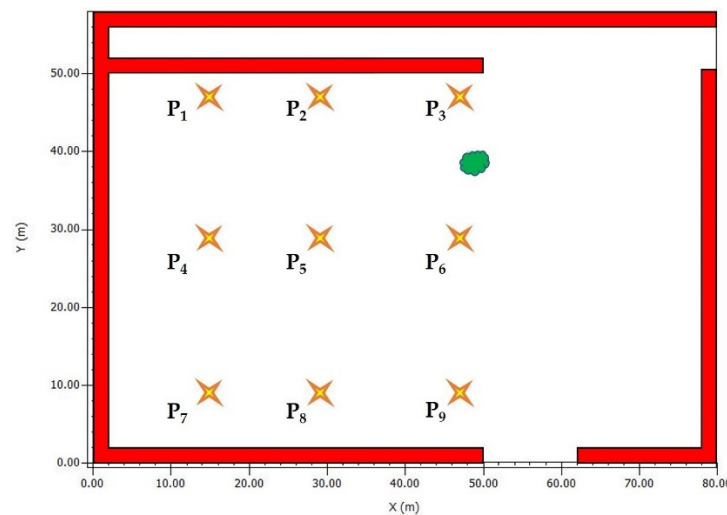
Figure 6. Layout of the ENVI-met model and the investigation points.

With regard to BI, Tables 6 and 7 list the AT values in P_i for each month of 2021 at 06:00 a.m. and 4:00 p.m., respectively. Such hours have been chosen because they are statistically the hours when the minimum and maximum AT occur. For each month, the statistical evaluations in terms of the P_i maximum, minimum, and average monthly AT (T_{max}, T_{min}, and T_{med}, respectively), and standard deviation (σ) values of AT allowed a simplification of the problem analysis.

In the early morning (Table 6), the monthly AT values of P_i highlight slight differences between T_{max} and T_{min} (up to 0.9 °C); σ ranges between 0.22 °C and 0.39 °C, with the highest values in summer. The statistical parameters show that once the month and the time of observation have been set, the AT does not vary significantly in the whole parking area.

Table 6. Air temperature at 06:00 a.m. in 2021—Scenario BI.

Month	AT (°C)									T_{max} (°C)	T_{min} (°C)	T_{med} (°C)	σ (°C)
	P_1	P_2	P_3	P_4	P_5	P_6	P_7	P_8	P_9				
Jan	4.90	4.91	4.89	5.20	5.24	5.20	5.37	5.41	5.40	5.41	4.89	5.17	0.22
Feb	7.18	7.18	7.13	7.58	7.61	7.55	7.80	7.84	7.81	7.84	7.13	7.52	0.29
Mar	6.41	6.42	6.38	6.86	6.88	6.83	7.12	7.16	7.13	7.16	6.38	6.80	0.32
Apr	9.27	9.28	9.24	9.67	9.71	9.66	9.91	9.96	9.94	9.96	9.24	9.63	0.29
May	14.26	14.27	14.21	14.67	14.71	14.66	14.92	14.97	14.93	14.97	14.21	14.62	0.30
Jun	19.53	19.52	19.41	20.04	20.06	19.99	20.34	20.38	20.32	20.38	19.41	19.95	0.38
Jul	22.44	22.42	22.27	22.94	22.97	22.89	23.23	23.29	23.22	23.29	22.27	22.85	0.39
Aug	23.20	23.18	23.01	23.65	23.68	23.60	23.89	23.96	23.89	23.96	23.01	23.56	0.35
Sep	19.34	19.32	19.14	19.83	19.85	19.76	20.09	20.15	20.08	20.15	19.14	19.73	0.38
Oct	13.22	13.20	13.08	13.66	13.68	13.60	13.60	13.94	13.89	13.94	13.08	13.54	0.31
Nov	10.77	10.77	10.68	11.08	11.11	11.05	11.22	11.27	11.25	11.27	10.68	11.02	0.23
Dec	6.01	6.01	5.96	6.36	6.38	6.33	6.54	6.58	6.56	6.58	5.96	6.30	0.25

Table 7. Air temperature at 04:00 p.m. in 2021—Scenario BI.

Month	AT (°C)									T_{max} (°C)	T_{min} (°C)	T_{med} (°C)	σ (°C)
	P_1	P_2	P_3	P_4	P_5	P_6	P_7	P_8	P_9				
Jan	10.02	10.17	10.43	9.63	9.80	9.97	9.45	9.56	9.74	10.43	9.45	9.86	0.31
Feb	13.94	14.15	14.60	13.42	13.65	13.95	13.23	13.37	13.71	14.60	13.23	13.78	0.43
Mar	14.31	14.63	15.41	13.64	13.99	14.62	13.46	13.76	14.30	15.41	13.46	14.24	0.61
Apr	17.15	17.59	18.26	16.30	17.02	17.50	16.25	16.86	17.20	18.26	16.25	17.13	0.63
May	22.50	22.87	23.58	21.61	22.40	22.85	21.65	22.26	22.53	23.58	21.61	22.47	0.61
Jun	29.20	29.56	30.27	28.32	29.05	29.49	28.34	28.87	29.10	30.27	28.32	29.13	0.61
Jul	32.08	32.46	33.14	31.16	31.91	32.36	31.15	31.71	31.96	33.14	31.15	31.99	0.63
Aug	31.90	32.31	32.95	31.02	31.78	32.23	30.96	31.57	31.85	32.95	30.96	31.84	0.62
Sep	28.06	28.48	29.02	27.31	27.69	28.30	27.10	27.43	27.93	29.02	27.10	27.92	0.61
Oct	20.67	20.91	21.32	20.13	20.37	20.62	20.62	20.04	20.32	21.32	20.04	20.55	0.40
Nov	15.92	16.05	16.27	15.52	15.71	15.86	15.34	15.45	15.63	16.27	15.34	15.75	0.30
Dec	11.68	11.79	12.00	11.23	11.40	11.53	11.01	11.12	11.27	12.00	11.01	11.45	0.33

The values in Table 7 confirm the trend observed in the early morning: in the hottest hours the AT values of P_i do not significantly differ; varying the month, σ ranges between 0.31 °C and 0.63 °C, and its highest values are in summer. Figure 7 shows the daily AT curves of P_5 (i.e., the central point in the parking lot in Figure 6) for each month. The curves describe the sinusoidal fluctuations in AT throughout the day: whatever the month, T_{min} is at 6:00 a.m., while the hour of T_{max} ranges between 3:00 p.m. (in the coldest months) and 4:00 p.m. (in the hottest months). Day–night temperature differentials are increasing from winter to summer.

Given the low differences between the calculated ATs of P_i in a set time (Tables 6 and 7), the authors decided to focus on the P_5 performances. Moreover, the statistical AT variables (i.e., T_{max}, T_{min}, T_{med}, and σ) at the critical hours during the day (Figure 7) have been considered to analyze the different scenarios. The comparison involved the results of the most critical months: they are January and December with regard to the lowest values of AT (Table 6), and July and August for the highest ones (Table 8).

As observed in Tables 4 and 5, σ values in Table 6 confirm the AT distribution over the parking lot does not depend on the chosen pavement material: they are 0.20–0.25 °C at 6:00 a.m. and 0.31–0.33 °C at 4:00 p.m. Given a time and a statistical temperature variable, in Table 6 the highest differences between the modeled scenarios range between 0.6 °C (for T_{min} at 6 a.m.) and 0.4 °C (for T_{med} at 4:00 p.m.). Comparable absolute values are for BI, LC, and BR at 6:00 a.m. (T_{med} 5.2 °C in January and 6.3 °C in December). GR is the coldest solution, both in the early morning and in the evening; the hottest solution is SP at 6:00 a.m. and BI at 4:00 p.m.
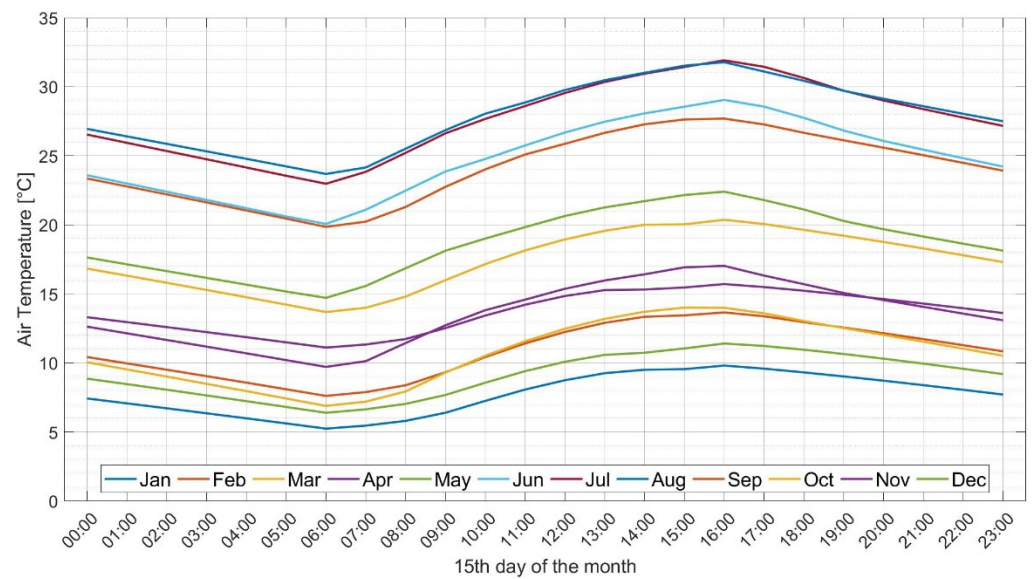
Figure 7. Daily AT curves of P_5—BI.

Table 8. Air temperature values at 06:00 a.m. and 04:00 p.m. in the coldest months of 2021.

Scenario	Month	06:00 a.m.				04:00 p.m.			
		T_{max} (°C)	T_{min} (°C)	T_{med} (°C)	σ (°C)	T_{max} (°C)	T_{min} (°C)	T_{med} (°C)	σ (°C)
BI	Jan	5.41	4.89	5.17	0.22	10.43	9.45	9.86	0.31
	Dec	6.58	5.96	6.30	0.25	12.00	11.01	11.45	0.33
LC	Jan	5.41	4.89	5.17	0.22	10.10	9.15	9.57	0.32
	Dec	6.59	5.97	6.31	0.25	11.74	10.78	11.22	0.33
BR	Jan	5.41	4.89	5.17	0.22	10.27	9.30	9.72	0.32
	Dec	6.59	5.96	6.31	0.25	11.87	10.90	11.34	0.33
SP	Jan	5.55	4.99	5.29	0.23	10.38	9.39	9.81	0.32
	Dec	6.72	6.09	6.43	0.26	11.95	10.96	11.40	0.33
WO	Jan	5.08	4.52	4.85	0.20	9.95	9.01	9.45	0.32
	Dec	6.27	5.60	6.00	0.24	11.61	10.66	11.11	0.33
GR	Jan	4.98	4.40	4.76	0.20	9.86	8.91	9.38	0.32
	Dec	6.16	5.47	5.89	0.23	11.47	10.53	11.01	0.33

Table 9 has σ values higher than those in Table 8; although they do not exceed 0.7 °C. However, σ values at 6:00 a.m. are lower than those in the evening. Given a time and a statistical temperature variable, in Table 9 the absolute differences between the modeled scenarios range between 0.7 °C (for T_{med} at 6 a.m.) and 1.6 °C (for T_{max} at 4:00 p.m.). The appreciable differences between AT values in the evening prove that a proper pavement material can counter the UHI effects. In particular, LC is the best solution (T_{max} 31.5 °C in July and August), slightly better than WO (31.7 °C in July and August). The hottest scenario is the current one (BI) with a T_{max} of 33.14 °C in July.

Figure 8 shows the daily AT curve of P_5 varying the parking lot pavement during January and August.

In Figure 8 the daily AT curves of BI and GR are comparable and differ from the other scenarios due to the thermal properties of the materials; since they have equal and low values of albedo (Tables 1 and 2), they heat up more than the others that have higher values of reflectivity. Due to the lower solar radiation, the curves of January are flatter than those in August. This reason justifies the hour when there is a breakeven point between the coldest and the hottest scenarios: in January it is at 9:00 a.m. and in August it is at 7:00 a.m. The analysis of the different curves in Figure 8 (gray curve) demonstrates that LC is the

most effective solution against UHI in the examined square. However, to pursue a holistic approach, the PMV trend has been analyzed to compare the scenarios. With regard to the current condition BI, Figure 9 shows the daily PMV curve of P_5.

Table 9. Air temperature values at 06:00 a.m. and 04:00 p.m. in the hottest months of 2021.

| Scenario	Month	06:00 a.m.				04:00 p.m.			
		T_{max} (°C)	T_{min} (°C)	T_{med} (°C)	σ (°C)	T_{max} (°C)	T_{min} (°C)	T_{med} (°C)	σ (°C)
BI	Jul	23.29	22.27	22.85	0.39	33.14	31.15	31.99	0.63
	Aug	23.96	23.01	23.56	0.35	32.95	30.96	31.84	0.62
LC	Jul	23.12	22.14	22.71	0.37	31.50	29.74	30.47	0.56
	Aug	23.83	22.91	23.45	0.34	31.48	29.80	30.51	0.54
BR	Jul	23.23	22.23	22.80	0.38	32.35	30.47	31.25	0.59
	Aug	23.91	22.98	23.53	0.34	32.24	30.41	31.20	0.57
SP	Jul	23.46	22.42	23.00	0.41	32.55	30.72	31.46	0.58
	Aug	24.11	23.16	23.70	0.36	32.43	30.62	31.38	0.56
WO	Jul	22.97	21.97	22.56	0.36	31.72	29.92	30.66	0.57
	Aug	23.70	22.76	23.33	0.33	31.70	29.96	30.69	0.55
GR	Jul	22.69	21.68	22.31	0.35	32.64	30.46	31.46	0.68
	Aug	23.41	22.44	23.05	0.32	32.43	30.29	31.29	0.67
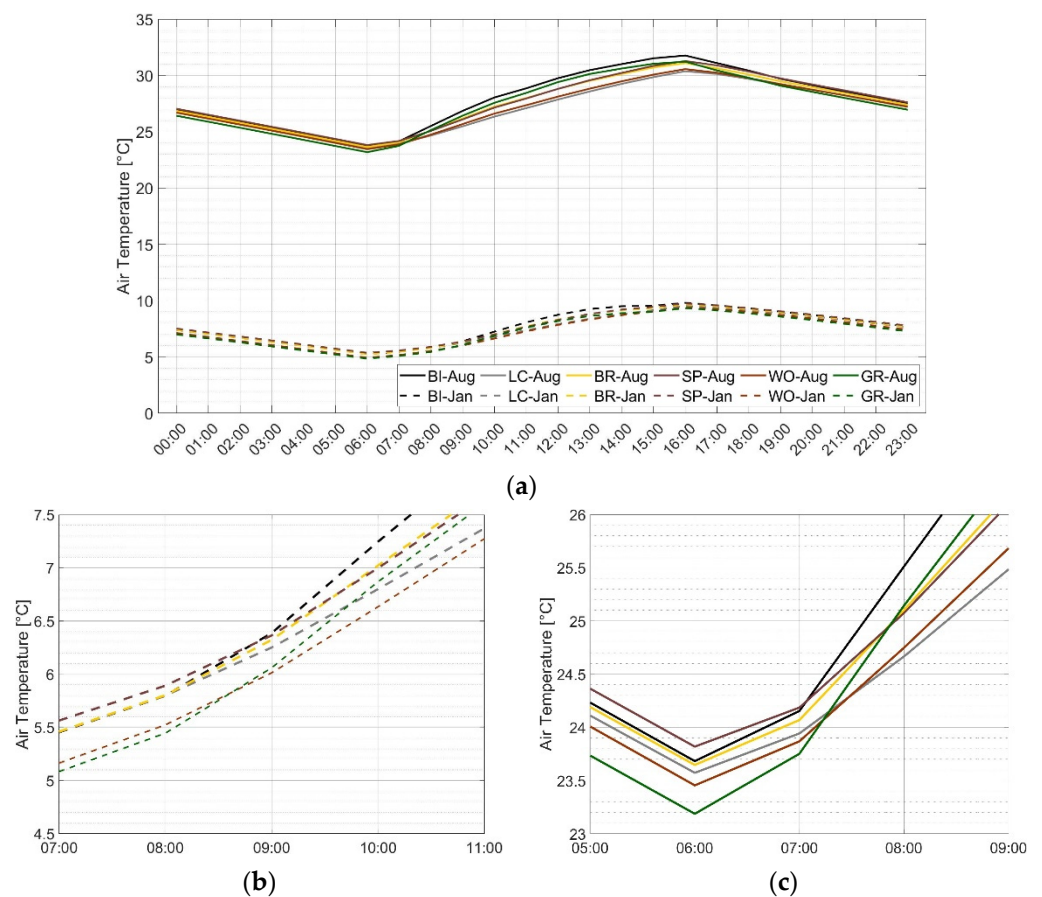
Figure 8. Daily AT curves of P_5. January and August. (**a**) 24 h curves; (**b**) detail of January 7:00 a.m.–11:00 a.m.; (**c**) detail of August 5:00 a.m.–9:00 a.m.
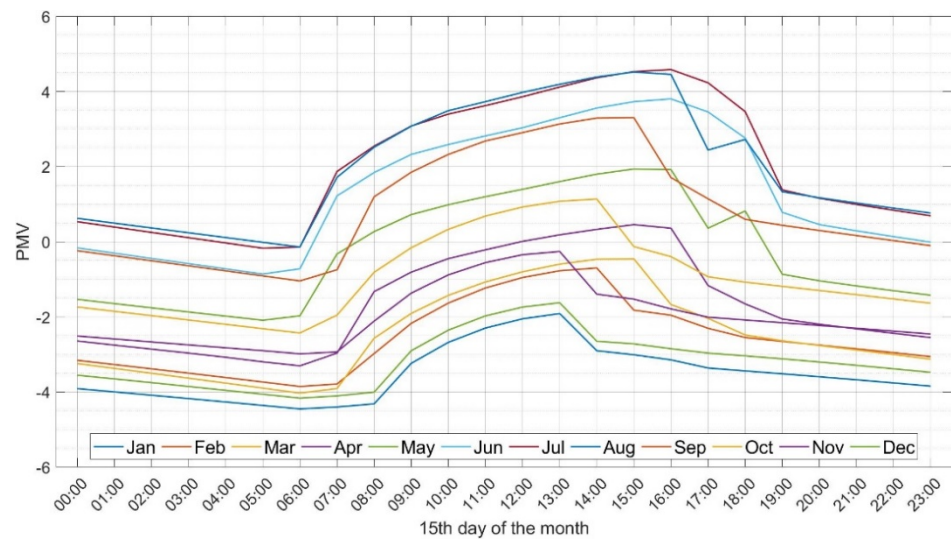
Figure 9. Daily PMV curves of P$_5$—BI.

According to the PMV scale in Figure 4, Figure 9 shows critical conditions to be deepened: the curves of both cold and hot months overcome the comfort zone. In particular, the lower and upper PMV curves refer to January and July, respectively. Therefore, the critical months vary with the physical parameter considered in the analysis: January is the most critical cold month in terms of both AT and PMV, while the most critical hot month is August in terms of AT and July in terms of PMV. The anomalous trend in May and June curves is due to local conditions; as shown in Figure 6, the square is surrounded by buildings of different heights, that, with their shadows, play an important role in the range of values assumed by AT and PMV in the analyzed spatial domain. The anomalies mentioned for May and June are due to the shadow of the bell tower located in the West corner of the square. Indeed, during the sunset, the tower causes a shadow on the P$_5$ area.

Figures 10 and 11 compare the daily PMV curves of P$_5$ for different scenarios in January and July, respectively.

The PMV values in January at 6:00 a.m. are: −4.41, −4.45, −4.45, −4.45, −4.54, and −4.55 for SP, BR, LC, BI, GR, and WO. The PMV values in January at 1:00 p.m. are: −1.91, −1.97, −1.99, −2.02, −2.04, and −2.16 for BI, BR, SP, LC, WO, and GR.

The PMV values in July at 5:00 a.m. are: −0.12, −0.17, −0.18, −0.21, −0.26, and −0.28 for SP, BI, BR, LC, WO, and GR, respectively. The PMV values in July at 4:00 p.m. are: 4.58, 4.50, 4.49, 4.43, 4.41, and 4.37 for BI, SP, BR, WO, GR, and LC, respectively. Finally, this study proposed an objective interpretation of the daily PMV curves in Figures 11 and 12: the integration with respect to the hour between ideal (IC), acceptable (AC), and critical (CC) PMV intervals. Tables 10 and 11 list the results of the PMV analysis of P$_5$ for January and July, respectively.

According to the results of Tables 10 and 11, the integration of the daily PMV curves show the best scenario for the whole day (i.e., SP in January and LC in July). However, the quantitative comparison between the different pavements with the evaluation of the distribution of the PMV in the whole square to a fixed hour has been continued. Indeed, the study of PMV focused on its distribution over the modeled square. Figure 12a–f shows the extreme results of the coldest hour (6:00 a.m.) of January for the scenarios BI, LC, BR, SP, WO, and GR, respectively. All of the scenarios give only critical conditions (Table 10) because their PMV values are less than −3. Small differences are between the lowest PMV values (below −4.72 in WO and GR) and the highest ones (above −4.38 in BI, LC, BR, and SP).
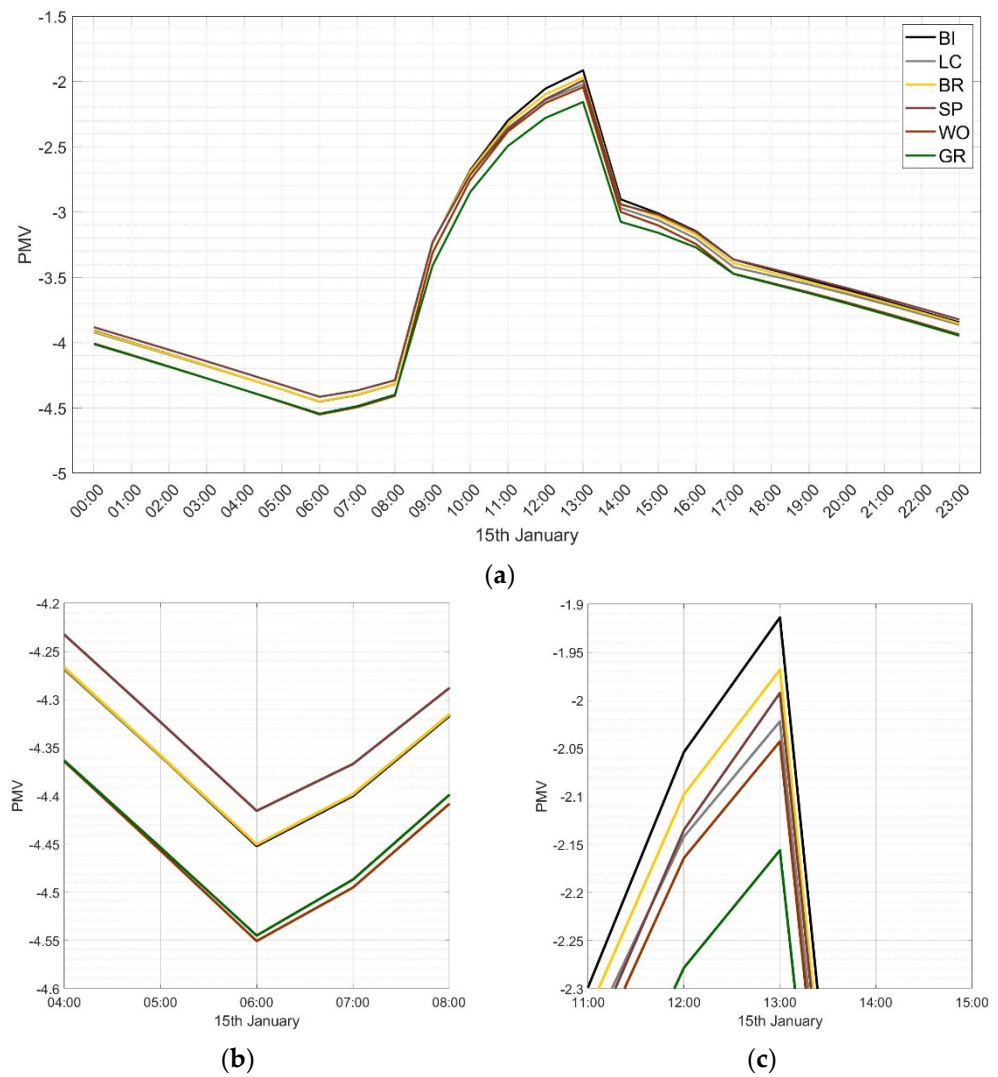
Figure 10. Daily PMV curves of P₅—January. (**a**) 24 h curves; (**b**) detail between 4:00 a.m.–8:00 a.m.; (**c**) detail between 11:00 a.m.–3:00 p.m. (3:00 p.m. is 15:00).
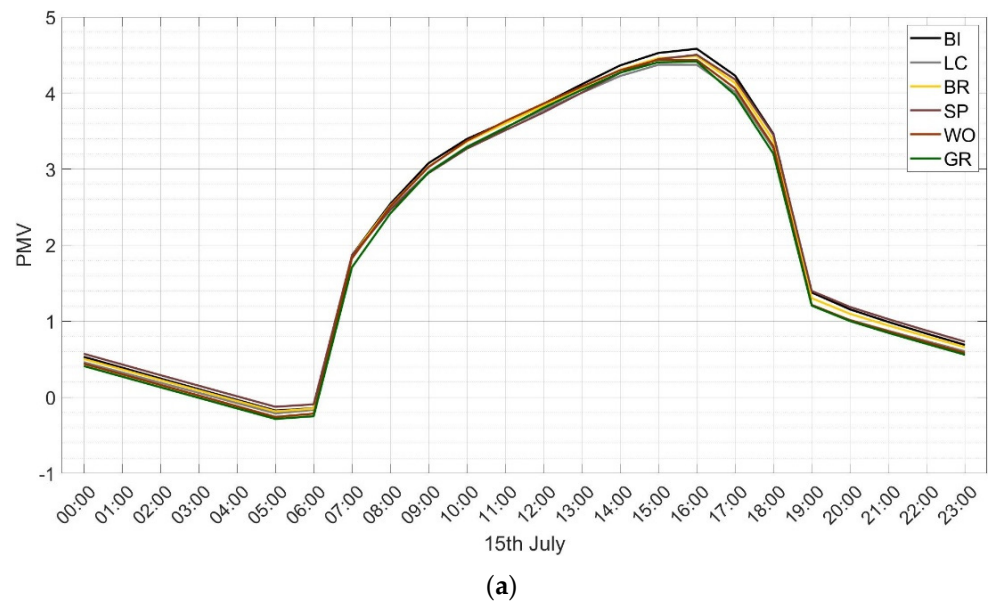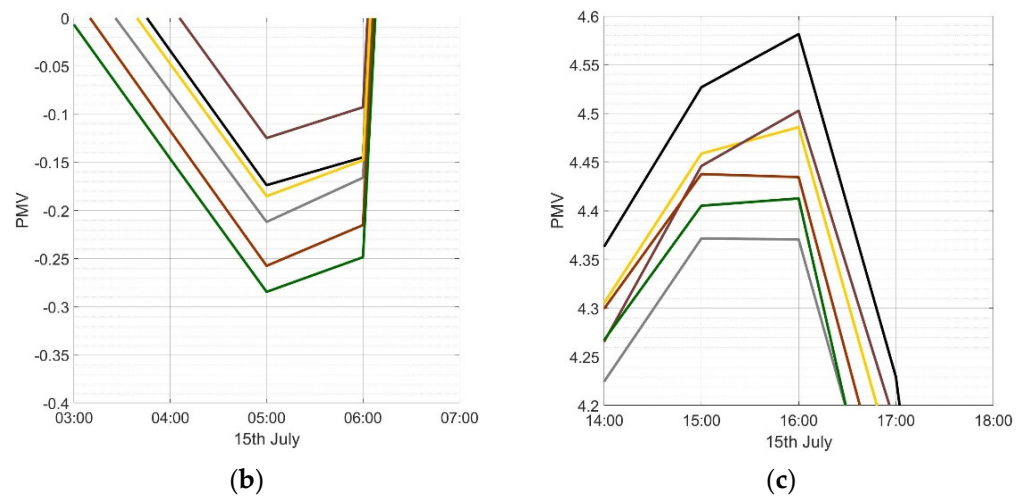

Figure 11. *Cont.*

(**b**)   (**c**)

Figure 11. Daily PMV curves of P$_5$—July. (**a**) 24 h curves; (**b**) detail between 3:00 a.m.–7:00 a.m.; (**c**) detail between 14:00 a.m.–18:00 a.m.
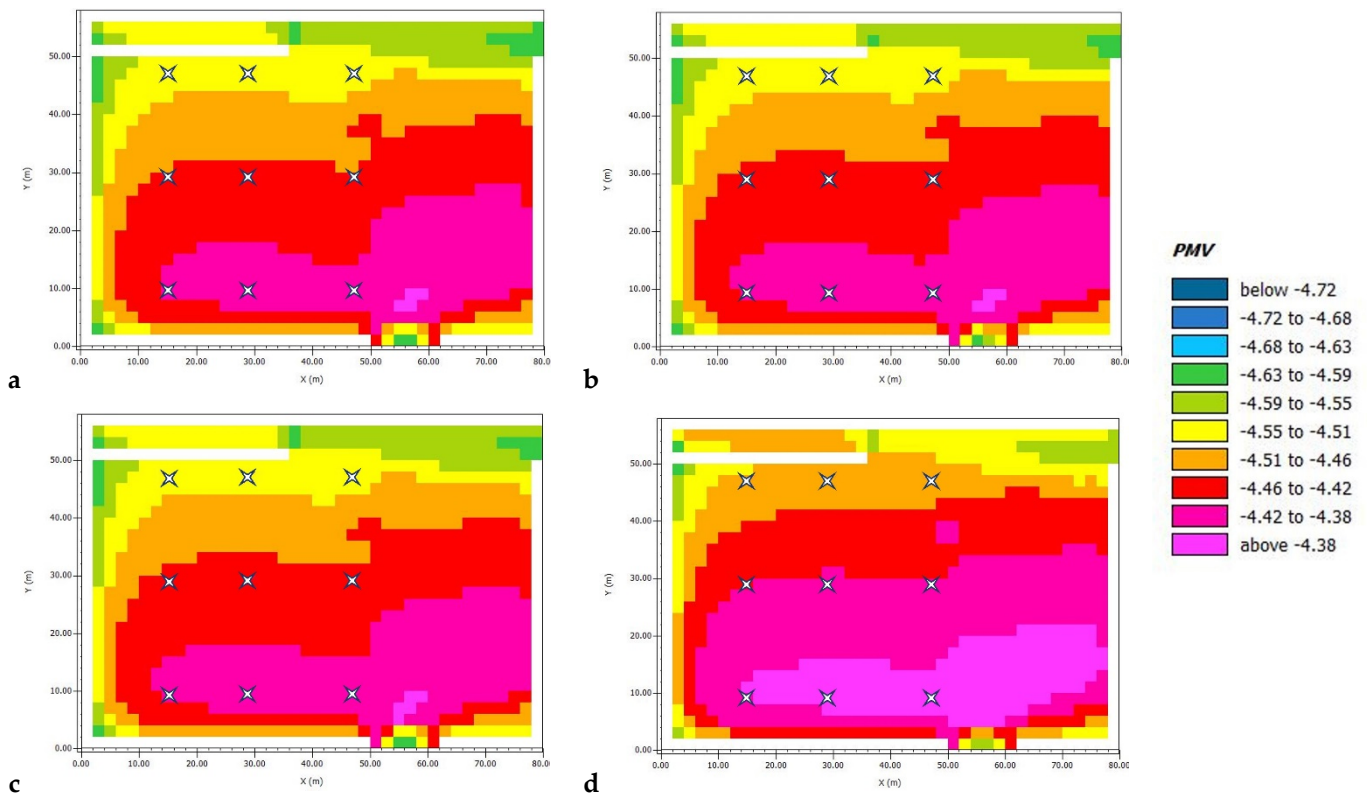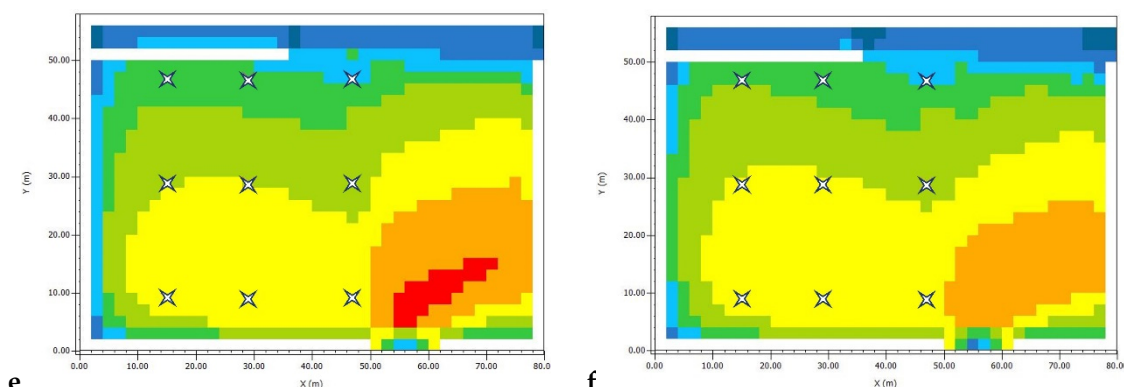

Figure 12. *Cont*.

Figure 12. PMV at 6:00 a.m. in January. (**a**) BI; (**b**) LC; (**c**) BR; (**d**) SP; (**e**) WO; (**f**) GR.

Table 10. PMV analysis of P_5—January.

January	PMV ≤ -3	$-3 <$ PMV < -1	$-1 \leq$ PMV ≤ 1	$1 <$ PMV < 3	PMV ≥ 3
	(PMV $\times$ h)	(PMV $\times$ h)	(PMV $\times$ h)	(PMV $\times$ h)	(PMV $\times$ h)
BI	14.61	42.92	23.00	0.00	0.00
LC	14.96	43.26	23.00	0.00	0.00
BR	14.76	43.09	23.00	0.00	0.00
SP	14.26	43.22	23.00	0.00	0.00
WO	16.33	43.41	23.00	0.00	0.00
GR	16.80	43.86	23.00	0.00	0.00

Table 11. PMV analysis of P_5—July.

July	PMV ≤ -3	$-3 <$ PMV < -1	$-1 \leq$ PMV ≤ 1	$1 <$ PMV < 3	PMV ≥ 3
	(PMV $\times$ h)	(PMV $\times$ h)	(PMV $\times$ h)	(PMV $\times$ h)	(PMV $\times$ h)
BI	0	0	17.63	22.91	9.02
LC	0	0	17.25	22.39	7.74
BR	0	0	17.49	22.69	8.49
SP	0	0	17.97	22.65	8.17
WO	0	0	18.22	22.46	8.37
GR	0	0	18.13	22.55	7.83

Figure 13a–f shows the extreme results of the hottest hour (4:00 p.m.) of July for the scenarios BI, LC, BR, SP, WO, and GR, respectively. As for AT, in the hottest month, the pavement choice significantly affects human comfort: PMV values range between acceptable (below 2.93) and critical (above 4.71) values. In particular, the chromatic representation of the results allows qualitative comparison between the perceived comfort.

Table 12 lists the percentage distribution of the modeled square's area falling in the different ideal (IC), acceptable (AC), and critical (CC) PMV intervals, according to the two-dimensional colored maps in Figures 12 and 13. The results in Tables 11 and 12 show a discrepancy in the best scenario to ensure good thermal comfort. In detail, in 24 h, the existing pavement (BI) is the worst, while concrete blocks (LC) are the best in P_5 (Table 11). Instead, analyzing the whole square in the critical hour of the hottest month of the year the parking area with grass (GR) is the best scenario because 16% of the square ensures PMV acceptable conditions.
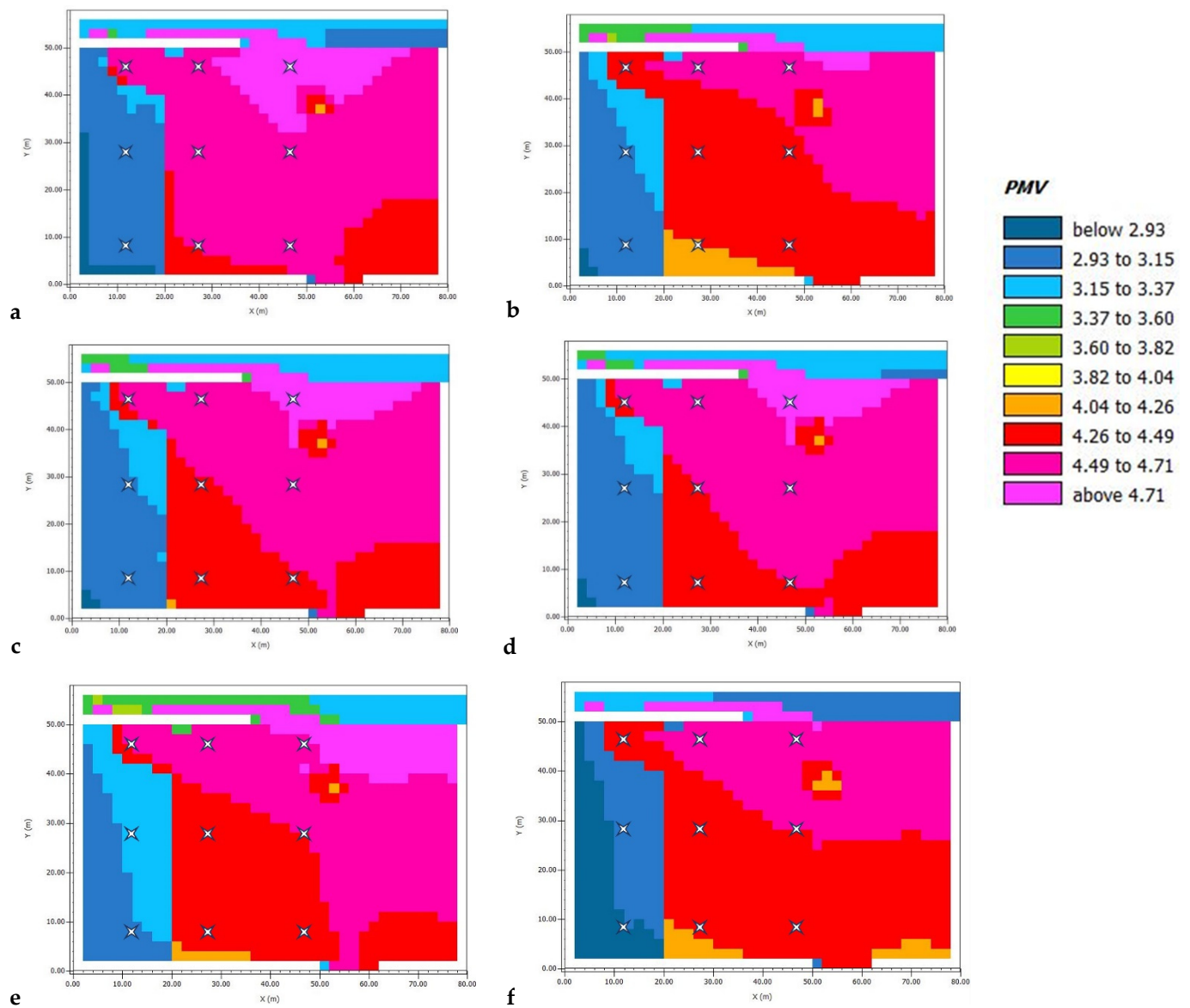
Figure 13. PMV at 4:00 p.m. in July. (**a**) BI; (**b**) LC; (**c**) BR; (**d**) SP; (**e**) WO; (**f**) GR.

Table 12. Percentage distribution of PMV values.

Scenario	Month	Percentage Distribution of PMV Values (%)				
		PMV ≤ −3	−3 < PMV < −1	−1 ≤ PMV ≤ 1	1 < PMV < 3	PMV ≥ 3
BI	January	100	0	0	0	0
	July	0	0	0	5	95
LC	January	100	0	0	0	0
	July	0	0	0	3	97
BR	January	100	0	0	0	0
	July	0	0	0	3	97
SP	January	100	0	0	0	0
	July	0	0	0	4	96
WO	January	100	0	0	0	0
	July	0	0	0	1	99
GR	January	100	0	0	0	0
	July	0	0	0	16	84

4. Discussion

The proposed study defined a methodology that allows the definition of the best cool pavement able to mitigate the negative effect of UHIs in an Italian square. The analysis compared the existing scenario to five other solutions, obtained by replacing the asphalt layer of the parking lot with different cool materials. The existing scenario has been modeled in ENVI-met and validated through in situ measurements of air temperature, relative humidity, and wind speed. These parameters have been measured three times in a year (July, October, and February). The estimation of the climatic variables gave acceptable RMSE values: in the worst condition they are 0.16 °C, 19.3%, and 0.62 m/s. To make a correct and detailed assessment of the best scenario, a simulation of the whole year of 2021 was performed. The investigation focused on two variables examined (i.e., air temperature and PMV) in the cold and hot critical months. Nine survey points (Figure 6) have been defined to monitor the trends of the two variables in the examined parking lot. The statistical analysis of the thermal performances highlighted there are non-large differences between the detected values: at a set time the thermal response of the square can be considered constant.

The results in terms of AT and PMV showed that there is not an absolute best solution, but that there are different acceptable solutions that depend on the critical cold/hot month and the examined variables.

In the case of AT, the critical hot and cold months were August and January, respectively; the daily AT trends showed that LC is the best solution against UHI for the examined square. In August, during the morning, the LC records an AT value of 0.4 °C less than the value recorded by the grass pavement, instead, at 04:00 p.m. the values are reversed, and LC records an AT equal to 31.2 °C, while GR is 30.4 °C.

For the PMV index, the cold critical month was January, while the hottest one, unlike the AT values, was July. Even for the PMV values, in July, during the morning, the LC records a PMV value of 0.07 more than the value recorded by the grass pavement, instead, at 03:00 p.m. the values are reversed, and LC records a PMV equal to 4.31, while GR is 4.37. By the scientific literature, three different conditions are defined according to the PMV values: IC, AC, and CC. For this reason, the authors proposed a methodology to evaluate the best pavement in terms of PMV based on the values' distribution of the same index in the three different ranges. The results showed that daily LC is the best solution because it exposes the square to the worst condition (CC) for the shortest time. On the other hand, the analysis of the colored maps from ENVI-met showed that the best solution in the hottest hour of July is the GR (i.e., a green layer over the parking lot). Therefore, the proposed methodology allows for a 24 h analysis and overcomes a punctual approach that focuses only on the extreme peak values.

The results confirm that UHIs are also influenced by the surface material adopted to pave roads and the existing asphalt scenario is the worst one both for AT and PMV values. The use of cool pavements can instead guarantee a human perception of comfort. Finally, especially for the PMV values, the results show that LC and GR are the two best solutions. These results are closely related to the local conditions of each specific site, such as the LAT/LONG on which solar radiation depends, the buildings surrounding the studied area, the thermal properties of the material used, and, of course, other pavement materials that cannot be considered in this study due to the planning restriction and the Italian guidelines.

Further analyses should be carried out to improve the obtained results by adding vegetation (e.g., trees and hedges) in the parking lot with LC and GR.

5. Conclusions

The evolution of global warming is causing continuous climate change and the consequent increase in temperatures, which negatively affect human living comfort. The anthropological use of soil causes the phenomenon of UHIs because impermeable artificial surfaces substitute the natural ones. Several scientific studies have sought to identify the best mitigation methods to counter UHIs by proposing the use of green infrastructures

(e.g., green roofs, green walls, green corridors, and green networks) and the replacement of existing road pavements with cool ones (e.g., stone, light concrete, and grass). Compared to the traditional asphalt pavements, cool pavements are composed of alternative materials with high albedo. Such physical property results in a lowering of the diurnal surface temperature and a reduction in the absorbed heat. A three-dimensional microclimatic analysis was carried out using the ENVI-met 3.4 LITE software. The effects of the surrounding environment, such as vegetation, urban fabric, and weather conditions have been modeled. The existing asphalt pavement and five other scenarios, differentiated by different materials (i.e., light concrete, brick, stone, wood, and grass) have been modeled to characterize St. Peter in Chains' square in Rome during the year 2021. The reported validation results of the current scenario confirmed the reliability of the model: RMSE values in the worst condition are 0.16 °C, 19.3%, and 0.62 m/s. The climatic variables have been measured three times in a year (July, October, and February). Therefore, this study carried out a survey to define a methodology to investigate the environmental conditions and mitigate the consequences of climate change.

The results allowed for a comparison between the different pavements, identifying for each of them the improvement in terms of AT and PMV compared to the existing scenario, which is the worst. The proposed methodology has identified that the replacement of the existing pavement with light concrete blocks leads to the greatest improvements both in terms of AT and PMV. In the hottest month (e.g., August), the maximum evening AT values are: 33.1 °C, 31.5 °C, 32.4 °C, 32.6 °C, 31.7 °C, and 32.7 °C for BI, LC, BR, SP, WO, and GR, respectively. On the other hand, the PMV values in July at 04:00 p.m. are: 4.58, 4.50, 4.49, 4.43, 4.41, and 4.37 for BI, SP, BR, WO, GR, and LC. These results show that there is not an absolute best scenario in terms of cool pavement materials, but there are different acceptable options based on the critical cold/hot month and the examined variables. The outcome of this research suggests that merging the two best scenarios (LC and GR) could make an even greater contribution to UHI mitigation, by inserting more vegetation into the square (e.g., trees and hedges). To preserve the existing historical and cultural constraints of the site, further analyses should be carried out to identify a compromise between heritage and wellbeing. In conclusion, the proposed study showed how cool pavement can be defined as an excellent strategy to improve the perceived state of thermal human comfort.

References

1. Wit, S.; Haines, S. Climate Change Reception Studies in Anthropology. *WIREs Clim. Chang.* **2022**, *13*, e742. [CrossRef]
2. Agrawal, N.; Pandey, V.K.; Mishra, S.K.; Pandey, V.S. Modeling Seasonal Trends in Optimum Temperatures over India. *J. Water Clim. Chang.* **2021**, *12*, 1420–1436. [CrossRef]
3. Paltsev, S.; Monier, E.; Scott, J.; Sokolov, A.; Reilly, J. Integrated Economic and Climate Projections for Impact Assessment. *Clim. Chang.* **2015**, *131*, 21–33. [CrossRef]

4. Fathi, S.; Sajadzadeh, H.; Sheshkal, F.M.; Aram, F.; Pinter, G.; Felde, I.; Mosavi, A. The Role of Urban Morphology Design on Enhancing Physical Activity and Public Health. *Int. J. Environ. Res. Public Health* **2020**, *17*, 2359. [CrossRef]

5. Faroughi, M.; Karimimoshaver, M.; Aram, F.; Solgi, E.; Mosavi, A.; Nabipour, N.; Chau, K.W. Computational modeling of landsurface temperature using remote sensing data to investigate the spatial arrangement of buildings and energy consumption relationship. *Eng. Appl. Comput. Fluid Mech.* **2020**, *14*, 254–270. [CrossRef]

6. Mohajerani, A.; Bakaric, J.; Jeffrey-Bailey, T. The Urban Heat Island Effect, Its Causes, and Mitigation, with Reference to the Thermal Properties of Asphalt Concrete. *J. Environ. Manag.* **2017**, *197*, 522–538. [CrossRef]

7. Santamouris, M. Using Cool Pavements as a Mitigation Strategy to Fight Urban Heat Island—A Review of the Actual Developments. *Renew. Sustain. Energy Rev.* **2013**, *26*, 224–240. [CrossRef]

8. Cantelli, A.; Monti, P.; Leuzzi, G. Influence of the Urban Heat Island Parameterization on Precipitation Forecasting in Limited Area Model. In *Environmental Hydraulics*; CRC Press: Boca Raton, FL, USA, 2010; pp. 1151–1156.

9. Ravanelli, R.; Nascetti, A.; Cirigliano, R.V.; Di Rico, C.; Leuzzi, G.; Monti, P.; Crespi, M. Monitoring the Impact of Land Cover Change on Surface Urban Heat Island through Google Earth Engine: Proposal of a Global Methodology, First Applications and Problems. *Remote Sens.* **2018**, *10*, 1488. [CrossRef]

10. Pomerantz, M.; Pon, B.; Akbari, H.; Chang, S.-C. *The Effect of Pavements Temperatures on Air Temperatures in Large Cities*; LNBL-43442; Lawrence Berkeley National Laboratory: Berkeley, CA, USA, 2000.

11. Vujovic, S.; Haddad, B.; Karaky, H.; Sebaibi, N.; Boutouil, M. Urban Heat Island: Causes, Consequences, and Mitigation Measures with Emphasis on Reflective and Permeable Pavements. *CivilEng* **2021**, *2*, 459–484. [CrossRef]

12. Cantelli, A.; Monti, P.; Leuzzi, G. An Investigation of the Urban Heat Island of Rome through a Canyon-Based Subgrid Scheme. *Int. J. Environ. Pollut.* **2011**, *47*, 239–247. [CrossRef]

13. Wong, E. Reducing urban heat islands: Compendium of strategies—Urban heat island basics. In *The Climate Protection Partnership Division*; Environmental Protection Agency's Office of Atmospheric Programs: Washington, DC, USA, 2014.

14. Killingsworth, B.; Lemay, L.; Peng, T. *Concrete's Role in Reducing Urban Heat Islands*; Concrete Sustainability Report; NRMCA CSR: Alexandria, VA, USA, 2014.

15. MacLachlan, A.; Biggs, E.; Roberts, G.; Boruff, B. Urbanisation-Induced Land Cover Temperature Dynamics for Sustainable Future Urban Heat Island Mitigation. *Urban Sci.* **2017**, *1*, 38. [CrossRef]

16. Cheela, V.R.S.; John, M.; Biswas, W.; Sarker, P. Combating Urban Heat Island Effect—A Review of Reflective Pavements and Tree Shading Strategies. *Buildings* **2021**, *11*, 93. [CrossRef]

17. Akpınar, M.V.; Sevin, S. Reducing Urban Heat Islands by Developing Cool Pavements. In *The Role of Exergy in Energy and the Environment*; Nižeti'c, S., Papadopoulos, A., Eds.; Green Energy and Technology; Springer: Cham, Switzerland, 2018. [CrossRef]

18. Akbari, H.; Rose, L.S. Urban Surfaces and Heat Island Mitigation Potentials. *J. Hum.-Environ. Syst.* **2008**, *11*, 85–101. [CrossRef]

19. Ibrahim, S.H.; Ibrahim, N.I.A.; Wahid, J.; Goh, N.A.; Koesmeri, D.R.A.; Nawi, M.N.M. The impact of road pavement on urban heat island (UHI) phenomenon. *Int. J. Technol.* **2018**, *9*, 1597–1608. [CrossRef]

20. Norton, B.A.; Coutts, A.M.; Livesley, S.J.; Harris, R.J.; Hunter, A.M.; Williams, N.S.G. Planning for Cooler Cities: A Framework to Prioritise Green Infrastructure to Mitigate High Temperatures in Urban Landscapes. *Landsc. Urban Plan.* **2015**, *134*, 127–138. [CrossRef]

21. Costanzo, V.; Evola, G.M. Energy savings in buildings or UHI mitigation? Comparison between green roofs and cool roofs. *Energy Build.* **2016**, *114*, 247–255. [CrossRef]

22. Ranieri, V.; Coropulis, S.; Berloco, N.; Fedele, V.; Intini, P.; Laricchia, C.; Colonna, P. The Effect of Different Road Pavement Typologies on Urban Heat Island: A Case Study. *Sustain. Resilient Infrastruct.* **2022**, 1–20. [CrossRef]

23. Lin, B.B.; Meyers, J.; Beaty, R.M.; Barnett, G.B. Urban Green Infrastructure Impacts on Climate Regulation Services in Sydney, Australia. *Sustainability* **2016**, *8*, 788. [CrossRef]

24. Senosiain, J.L. Urban Regreeneration: Green Urban Infrastructure as a Response to Climate Change Mitigation and Adaptation. *Int. J. Des. Nat. Ecodynamics* **2020**, *15*, 33–38. [CrossRef]

25. Francis, L.F.M.; Jensen, M.B. Benefits of Green Roofs: A Systematic Review of the Evidence for Three Ecosystem Services. *Urban For. Urban Green.* **2017**, *28*, 167–176. [CrossRef]

26. Adwan, I.; Milad, A.; Memon, Z.A.; Widyatmoko, I.; Zanuri, N.A.; Memon, N.A.; Yusoff, N.I.M. Asphalt Pavement Temperature Prediction Models: A Review. *Appl. Sci.* **2021**, *11*, 3794. [CrossRef]

27. Thai, H.N.; Kawamoto, K.; Nguyen, H.G.; Sakaki, T.; Komatsu, T.; Moldrup, P. Measurements and Modeling of Thermal Conductivity of Recycled Aggregates from Concrete, Clay Brick, and Their Mixtures with Autoclaved Aerated Concrete Grains. *Sustainability* **2022**, *14*, 2417. [CrossRef]

28. Noro, M.; Lazzarin, R. Urban Climate Urban Heat Island in Padua, Italy: Simulation Analysis and Mitigation Strategies. *Urban Clim.* **2015**, *14*, 187–196. [CrossRef]

29. Akbari, H.; Matthews, H.D. Global Cooling Updates: Reflective Roofs and Pavements. *Energy Build.* **2012**, *55*, 2–6. [CrossRef]

30. Kappou, S.; Souliotis, M.; Papaefthimiou, S.; Panaras, G.; Paravantis, J.A.; Michalena, E.; Hills, J.M.; Vouros, A.P.; Ntymenou, A.; Mihalakakou, G. Cool Pavements: State of the Art and New Technologies. *Sustainability* **2022**, *14*, 5159. [CrossRef]

31. Croce, S.; Agnolo, E.D.; Caini, M.; Paparella, R. The Use of Cool Pavements for the Regeneration of Industrial Districts. *Sustainability* **2021**, *13*, 6322. [CrossRef]

32. Moretti, L.; Loprencipe, G. Climate Change and Transport Infrastructures: State of the Art. *Sustainability* **2018**, *10*, 4098. [CrossRef]

33. Sanjuán, M.Á.; Morales, Á.; Zaragoza, A. Effect of Precast Concrete Pavement Albedo on the Climate Change Mitigation in Spain. *Sustainability* **2021**, *13*, 11448. [CrossRef]

34. Xie, J.; Zhou, Z. Numerical Analysis on the Optimization of Evaporative Cooling Performance for Permeable Pavements. *Sustainability* **2022**, *14*, 4915. [CrossRef]

35. Sansalone, J.; Kuang, X.; Ranieri, V. Permeable Pavement as a Hydraulic and Filtration Interface for Urban Drainage. *J. Irrig. Drain. Eng.* **2008**, *134*, 666–674. [CrossRef]

36. Di Mascio, P.; Moretti, L.; Capannolo, A. Concrete Block Pavements in Urban and Local Roads: Analysis of Stress-Strain Condition and Proposal for a Catalogue. *J. Traffic Transp. Eng.* **2019**, *6*, 557–566. [CrossRef]

37. Zoccali, P.; Moretti, L.; Di Mascio, P.; Loprencipe, G.; D'Andrea, A.; Bonin, G.; Teltayev, B.; Caro, S. Analysis of Natural Stone Block Pavements in Urban Shared Areas. *Case Stud. Constr. Mater.* **2018**, *8*, 498–506. [CrossRef]

38. Li, H.; Harvey, J.; Kendall, A. Field Measurement of Albedo for Different Land Cover Materials and Effects on Thermal Performance. *Build. Environ.* **2013**, *59*, 536–546. [CrossRef]

39. Senevirathne, D.; Jayasooriya, V.; Muthukumaran, S. A Study on Pedestrian Pavement Thermal Performance with Reference to Associated Materials. In Proceedings of the MERCon 2021—7th International Multidisciplinary Moratuwa Engineering Research Conference, Moratuwa, Sri Lanka, 27–29 July 2021; pp. 637–642. [CrossRef]

40. Italian Ministry of the Environment. *Adozione Dei Criteri Ambientali Minimi per l'Affidamento di Servizi di Progettazione e Lavori per la Nuova Costruzione, Ristrutturazione e Manutenzione di Edifici Pubblici*; Italian Ministry of the Environment: Rome, Italy, 2017.

41. Kusumastuty, K.D.; Poerbo, H.W.; Koerniawan, M.D. Climate-Sensitive Urban Design through Envi-Met Simulation: Case Study in Kemayoran, Jakarta. *IOP Conf. Ser. Earth Environ. Sci.* **2018**, *129*, 012036. [CrossRef]

42. Moretti, L.; Cantisani, G.; Carpiceci, M.; D'Andrea, A.; Del Serrone, G.; Di Mascio, P.; Loprencipe, G. Effect of Sampietrini Pavers on Urban Heat Islands. *Int. J. Environ. Res. Public Health* **2021**, *18*, 13108. [CrossRef]

43. Gilani, S.I.U.H.; Khan, M.H.; Pao, W. Thermal Comfort Analysis of PMV Model Prediction in Air Conditioned and Naturally Ventilated Buildings. *Energy Procedia* **2015**, *75*, 1373–1379. [CrossRef]

44. Ruiz, M.A.; Correa, E.N. Suitability of different comfort indices for the prediction of thermal conditions in tree-covered outdoor spaces in arid cities. *Theor. Appl. Climatol.* **2015**, *122*, 69–83. [CrossRef]

45. Chatzinikolaou, E.; Chalkias, C.; Dimopoulou, E. Urban microclimate improvement using Envi-met climate model. In Proceedings of the International Archives of the Photogrammetry, Remote Sensing and Spatial Information Sciences, Volume XLII-4, 2018 ISPRS TC IV Mid-term Symposium "3D Spatial Information Science–The Engine of Change", Delft, The Netherland, 1–5 October 2018. [CrossRef]

46. Wei, H.; Ke, X. Study of measurement and Envi-met simulation of winter night in NanPing Village under wet and cold microclimate based on urban roughness. In *PROJECTIONS, Proceedings of the 26th International Conference of the Association for Computer-Aided Architectural Design Research in Asia (CAADRIA), Hong Kong, China, 29 March–1 April 2021*; Association for Computer-Aided Architectural Design Research in Asia (CAADRIA): Hong Kong, China, 2021; Volume 2, pp. 427–436.

47. Romano, R.; Bologna, R.; Hasanaj, G.; Arnetoli, M.V. Adaptive design to mitigate the effects of UHI: The case study of Piazza Togliatti in the Municipality of Scandicci. In *Sustainability in Energy and Buildings*; Littlewood, J., Howlett, R., Capozzoli, A., Jain, L., Eds.; Smart Innovation, Systems and Technologies; Springer: Singapore, 2019; Volume 163. [CrossRef]

48. Liu, C.; Yuan, D. Temperature Distribution in Layered Road Structures. *J. Transp. Eng.* **2000**, *126*, 93–95. [CrossRef]

49. Wayne Lee, K.; Kohm, S. Cool Pavements as Sustainable Approaches for Green Streets and Highways. *Green Energy Technol.* **2014**, *204*, 439–453.

50. Coseo, P.; Larsen, L. Cooling the Heat Island in Compact Urban Environments: The Effectiveness of Chicago's Green Alley Program. *Procedia Eng.* **2015**, *118*, 691–710. [CrossRef]

51. Wijeyesekera, D.; Mohamad Nazari, N.A.; Lim, S.; Masirin, M.; Zainorabidin, A.; Walsh, J. Investigation Into the Urban Heat Island Effects From Asphalt Pavements. *OIDA Int. J. Sustain. Dev.* **2012**, *5*, 97–118.

52. Fiumi, L.; Georgiadis, T. Integrazioni di tecniche per la caratterizzazione termica delle pavimentazioni stradali in ambito urbano. In Proceedings of the Atti 12ª Conferenza Nazionale ASITA, L'Aquila, Italy, 21–24 October 2008. Available online: http://atti.asita.it/Asita2008/Pdf/233.pdf (accessed on 20 April 2022).

53. Progettare IL Comfort Degli Spazi Pubblici. Available online: https://territorio.regione.emilia-romagna.it/paesaggio/formazione-lab-app-1/rebus08-progettare-comfort-spazi-pubblici-valentina-dessi (accessed on 22 April 2022).

54. Tsoka, S.; Tsikaloudaki, A.; Theodosiou, T. Analyzing the ENVI-Met Microclimate Model's Performance and Assessing Cool Materials and Urban Vegetation Applications—A Review. *Sustain. Cities Soc.* **2018**, *43*, 55–76. [CrossRef]

55. Alvarez, I.; Quesada-Ganuza, L.; Briz, E.; Garmendia, L. Urban Heat Islands and Thermal Comfort: A Case Study of Zorrotzaurre Island in Bilbao. *Sustainability* **2021**, *13*, 6106. [CrossRef]

56. Fabbri, K.; Di Nunzio, A.; Gaspari, J.; Antonini, E.; Boeri, A. Outdoor Comfort: The ENVI-BUG Tool to Evaluate PMV Values Output Comfort Point by Point. *Energy Procedia* **2017**, *111*, 510–519. [CrossRef]

57. Moretti, L.; Di Mascio, P.; Fusco, C. Porous Concrete for Pedestrian Pavements. *Water* **2019**, *11*, 2105. [CrossRef]

58. d'Ambrosio Alfano, F.R.; Olesen, B.W.; Palella, B.I.; Pepe, D.; Riccio, G. Fifty Years of PMV Model: Reliability, Implementation and Design of Software for Its Calculation. *Atmosphere* **2020**, *11*, 49. [CrossRef]

59. Dyvia, H.A.; Arif, C. Analysis of thermal comfort with predicted mean vote (PMV) index using artificial neural network. *IOP Conf. Ser. Earth Environ. Sci.* **2021**, *622*, 01201. [CrossRef]

60. Balany, F.; Ng, A.W.; Muttil, N.; Muthukumaran, S.; Wong, M.S. Green Infrastructure as an Urban Heat Island Mitigation Strategy—A Review. *Water* **2020**, *12*, 3577. [CrossRef]

61. Baloloy, A.; Cruz, J.A.; Sta Ana, R.R.; Blanco, A.; Lubrica, N.V.M.; Valdez, C.J.; Bernardo, J.J. Modelling and simulation of potential future urbanization scenarios and its effect on the microclimate of lower session road, Baguio city. In Proceedings of the ISPRS Annals of the Photogrammetry, Remote Sensing and Spatial Information Sciences, 2020 XXIV ISPRS Congress (2020 edition), Nice, France, 31 August–2 September 2020; Volume V-4-2020.

62. Herath, H.M.P.I.K.; Halwatura, R.U.; Jayasinghe, G.Y. Evaluation of green infrastructure effects on tropical Sri Lankan urban context as an urban heat island adaptation strategy. *Urban For. Urban Green.* **2018**, *29*, 212–222. [CrossRef]

63. *ISO 7726*; Ergonomics of the Thermal Environment—Instruments for Measuring Physical Quantities, 2nd ed. International Standard ISO 7726:1998 from Technical Committee ISO/TC 159. ISO (International Standard Organization): Berlin, Germany, 1998.

64. Jeong, D.; Park, K.; Song, B.; Kim, G.; Choi, C.; Moon, B. Validation of ENVI-met PMV values by in-situ measurements. In Proceedings of the 9th International Conference on Urban Climate Jointly with 12th Symposium on the Urban Environment, Toulouse, France, 20–24 July 2015; pp. 20–24.

65. Cocci Grifoni, R.; Pierantozzi, M.; Tascini, S.; Passerini, G. Assessing the representativeness of thermal comfort in outdoor spaces. *WIT Trans. Ecol. Environ.* **2012**, *155*, 835–846.

66. Fanger, P.O. *Thermal Comfort: Analysis and Applications in Environmental Engineering*; R.E. Krieger Publishing Company: Malabar, FL, USA, 1982.

67. Yang, Y.; Zhang, X.; Lu, X.; Hu, J.; Pan, X.; Zhu, Q.; Su, W. Effects of Building Design Elements on Residential Thermal Environment. *Sustainability* **2018**, *10*, 57. [CrossRef]

68. *ANSI/ASHRAE 55-2004*; Thermal Environmental Conditions for Human Occupancy. ASHRAE (American Society of Heating, Refrigerating and Air-Conditioning Engineers, Inc.): Atlanta, GA, USA, 2004.

69. *UNI EN ISO 7730:2006*; Ergonomia Degli Ambienti Termici-Determinazione Analitica e Interpretazione Del Benessere Termico Mediante Il Calcolo Degli Indici PMV e PPD e Dei Criteri di Benessere Termico Locale. UNI (Ente Italiano di Normazione): Milano, Italy, 2006.

70. Alfano, G.; Cannistraro, G.; d'Ambrosio Alfano, F.R.; Rizzo, G. Notes on the Use of the Tables of Standard ISO 7730 for the Evaluation of the PMV Index. *Indoor Built Environ.* **1996**, *5*, 355–357. [CrossRef]